 doi:10.20944/preprints202206.0254.v1

Article

Numerical Study on the Effect of Deposits Layer on the Minimum Wall Thickness of Boiler Water Tube Under Different Operating Conditions

Ahmed S. Aljohani[1], Khaled I. Ahmed[2], Saeed Asiri[3] and Mohamed H. Ahmed [4,5]

[1] Saudi Electricity Co.; Eng.asaj@gmail.com
[2] Mechanical Engineering Department, K.A.CARE Energy Research and Innovation Center, King Abdulaziz University, Jeddah 21589, Saudi Arabia; kahmed@kau.edu.sa
[3] Department of Mechanical Engineering, King Abdulaziz University, Jeddah 21589, Saudi Arabia.; saeed@asiri.net
[4] Mechanical Engineering Department, King Abdulaziz University, Jeddah 21589, Saudi Arabia; e-mail@e-mail.com
[5] Department of Mechanical Engineering, Assiut University, Assiut 71516, Egypt; e-mail@e-mail.com
* Correspondence: Eng,asaj@gmail.com; Tel.: (+966 56 984 0315, ASA)

Abstract: Steam boiler has a significant role in the industrial sector. The failure in boiler tubes significantly reduces the availability of the plant. Furthermore, deposits on the inner tube wall contribute to such failure by changing the thermal resistance of the wall, which causes a significant increase in the tube wall's temperature and, consequently, lower allowable stress. The presented thermal-fluid model is developed for the water tube. The model is implemented using ANSYS FLUENT to estimate the wall maximum water tube wall temperature considering the deposits layer and then determine the minimum thickness of the tube wall via ASME standards to assure safe operation. The model is verified via a mesh independence test. The minimum tube thickness is recommended and justified given the thermo-mechanical performance of the water tubes at several operating loads of 50, 75, and 100 %. These loads are implemented by different convective heat transfer coefficients of flue gases under different deposit thicknesses, thermal conductivity, and flue gas temperature. The present work contributes to the literature by recommending the minimum thickness of the water wall tubes and highlighting the thermo-mechanical effect of the deposits on water tube resilience under different operating conditions.

Keywords: steam boiler; water tube; deposit layer; tube wall thickness; wall tube thermal conductivity; thermo-mechanical performance

1. Introduction

The increasing energy demand induces continuous development in creating new energy generation systems and enhances the existing ones to be more robust and reliable. One such technology is steam thermal power plants, which possess a remarkable share in energy production worldwide and contributes to several applications. The boiler is an essential component in a thermal power plant to generate steam, driving the turbine to produce power or direct it to subsystems for subsequent use, such as in the desalination plant and fuel heating systems.

The tubes in water tube boilers are subjected to several types of failure [1] caused by stress rupture, waterside and fireside corrosion [2] [3], fatigue [4], erosion [5], and lack of quality control. The main focus of the present work is the stress rupture, particularly in water tubes, caused by the overheating associated with being exposed to high temperatures and pressure that lead to tube failure. These conditions are induced in the short or long term. For example, the former is associated with decreasing cooling rate possibly attributed to complete or partial plugging, sudden shutdown of boiler circulating water

 doi:10.20944/preprints202206.0254.v1

pump, the rabid temperature increased during the start-up of the boiler evaporation of water in the liquid section, the increase of the overall thermal resistance due to deposits accumulation inside the tube. The visual examination of the ruptured wall presents with fish mouth appearance, usually in overheating conditions [6]. Taler, et al., (2019) described the plastic deformation in the rupture area shows deformation with elongated grains in the tube over a period during prolonged heat transfer. Sun & Yan, (2018) and Modliński, et al., (2019) further explained the impact of the difference in temperature conditions on either side of the tube displays variation in the appearance. It has been reported that the different temperatures on either side of the wall, hot wall (fireside) and cool wall demonstrated microstructural changes, especially more towards the hotter side ([7], [8]). Concurring, Munda, et al., (2018) stated that the fire side wall presented in the trials with partial degradation (spheroidization) of the lamellar structure mainly of iron carbide in pearlite colonies. The lamellar structure indicates the main driving force for change, excessive surface energy, which reduces the internal energy of the tube. Munda, et al., (2018) further pointed out that after the rupture of the tube, the rapid cooling causes a change in the structure and formation of bainite. However, Ardy & Bangun, (2019) and Dehnavi, et al., (2017) demonstrated that the substantial increase in the temperature lowers the yield stress of the metal. Thus, if the yield stress becomes equal to or less than the hoop stress of a metal tube at high temperature, the tube starts to deform, bulge, and thin.([9], [10]). Munda, et al., (2018) have studied the short-term overheating failure of a boiler water wall tube and examined the evolution of different microstructures during the failure through visual examination. They have concluded from the microstructure examination that the failure occurred due to overheating above the eutectoid temperature (lower critical temperature) of the tube material.

One solution to prevent overheating problems is enhancing the heat transfer through the tube wall to the water. Several researchers enhance the heat transfer by modifying the water tubes' inner surface area or inserting different shapes of obstructions inside tubes to induce more flow turbulence and mixings. More details can be found in the review articles [11]. Either way, considerable concerns exist regarding these techniques for the possible, increasing accumulation rate of deposits inside tubes.

The majority of the literature paid attention to enhancing the heat transfer through the pipes without considering the adverse effect of the accumulated deposits inside the tube on the thermal-mechanical consequences. Therefore, the main objectives addressed in the present work are the numerical investigation of the impact of deposits thickness and thermal conductivity inside tubes on the minimum thickness of the water tube for safe operation under different working loads; the influence the operating conditions such as flue gas temperature on the minimum thickness of the furnace water tube during the boiler lifetime.

Ansys software provides a suite to cover the entire range of physics, which enables virtual access to any field of engineering simulation, thereby permitting designing models to identify problems and functional processes. Conventional gas boilers have been shown to dissipate a high heat loss. Thus, the engineers designed a new type of boiler with thermal efficiency ([12], [13]). Regardless, the efficient boilers engineers continued to develop for minimizing complete heat loss and designed Ansys software that analyzes the internal water distribution within the heat exchanger([14], [13]. Thus, Sadik Kakaç, et al., (2020) pointed out that the engineers aim to improve the heat exchange coefficient within the tube to permit higher water flow velocity.

Furthermore, Hu, et al., (2014) added that the system predicts the fluid flow behaviour of water in the heat exchanger and throughout its distribution. In addition, Hu, et al., (2014) showed that the software supported the designing of the simulation model for the boiler with boundary conditions of heat transfer and heat loss in the system. Thus, using the software, several simulations were garnered over many years for a substantial improvement in the flow and heat exchanging behaviour of the boiler with the updated shape of the baffle.

Preprints (www.preprints.org) | NOT PEER-REVIEWED | Posted: 17 June 2022 doi:10.20944/preprints202206.0254.v1

The present paper has been organized into three main sections: introduction, methodology, and results and discussion. In the methodology section, the physical model of the simulation domain is described with corresponding used dimensions and material properties. Then, the numerical analysis is presented, including the governing equations, boundary conditions, and the minimum thickness estimation relations. Subsequently, numerical solutions are introduced, including numerical schemes, mesh independence tests, and turbulence model verification. Finally, in the last section, the results highlight the effect of the deposit layer thickness, thermal conductivity, and flue gas temperature under different working loads on the minimum thickness of the water tube wall.

2. Methodology

2.1. Physical Model

The present work focuses on the water tube boiler. Figure 1 shows a schematic of the different components of the water tube boiler. These are lower water drums where the water is introduced after passing through the economizer and upper steam drum where the steam is extracted and directed to the superheater section. Both drums are connected via water tubes, and the present work concentrates on the furnace section where the water remains in the liquid phase, as shown in Fig. 1a. The considered tube has the current dimensions shown in Fig. 1b in terms of tube length (L_p), outer pipe diameter (D_o), tube thickness (t_p), and deposit layer thickness (t_d). The water tubes are made from carbon steel seamless pipe (SA210 C), and different deposits layer are considered in the present work using a generic material with a variable range of thermal conductivity and thickness. Table 1 shows material properties for different types of deposits and their properties. The used material properties and driving dimensions for different parts are presented in Table 1. The length of the tubes and original thickness are 44.45 mm and 5.588 mm, respectively. The new thickness of the water tube is calculated according to the maximum allowable stress for the given pressure and temperature obtained using different thermal conductivity ranging between 0.625-12.5, representing the minimum and maximum thermal conductivity of the deposits shown in Table 1, while the thicknesses are based on deposit maximum loading of 40 mg/cm^2. The present work is focused on the water tubes in the furnace section and therefore is considered a single-phase with temperature-independent material properties at the average temperature of inlet water and saturation temperature at the working pressure. Note that pressure ranges from 180 to 210 bar; however, the operating pressure adopted in the present work is the highest of the applicable range, 210 bar, which is expected to result in higher stresses on the water tubes.

Preprints (www.preprints.org) | NOT PEER-REVIEWED | Posted: 17 June 2022 doi:10.20944/preprints202206.0254.v1

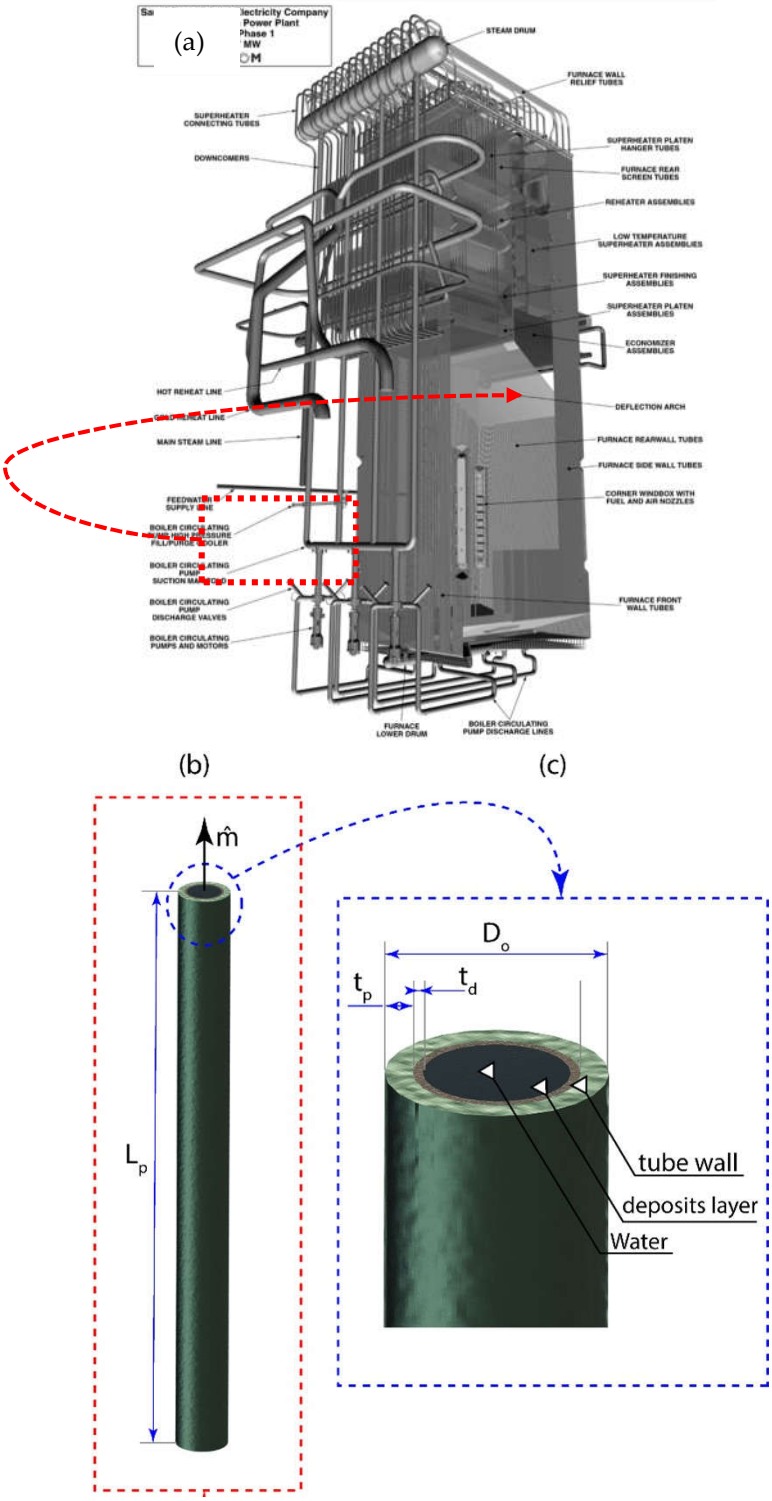

Figure 1. Schematic of (a) boiler ALSTOM Power 2000, (b) the simulated water tube, and (c) magnification of the tube tip with written parametric dimensions.

Preprints (www.preprints.org) | NOT PEER-REVIEWED | Posted: 17 June 2022 doi:10.20944/preprints202206.0254.v1

Table 1. Material properties commonly found in the deposits layer and the maximum allowable thickness based on maximum allowable deposits loading of $DP = 40\ mg/cm^3$.

Deposit material	Chemical Formula	Density kg/m³	Specific heat j/kg · K	Thermal conductivity W/m · K	Max. allowable thickness mm
Aragonite	$CaCO_3$	2930	785	2.1	0.137
Calcite	$CaCO_3$	2711	834.3	5.526	0.148
Anhydrite	$CaSO_4$	2320-2960	1130.436	1.5-7.5	0.135-0.172
Magnetite	Fe_3O_4	5175-2960	586	0.625-1.39	0.077
Hematite	Fe_2O_3	7874	6206	12.5	0.051
Quartz	SiO_2	2650	7406	11.7	0.151
Brucite	$Mg(OH)_2$	2380	77.03	8	0.168
Generic Range	-	5175	586	0.625-12.5*	0-0.172**

* refers to the tested range of thermal conductivity of generic deposits layer.
** represents the maximum thickness of the deposits layer at the maximum allowable deposits loading of $DP = 40\ mg/cm^3$

Table 2. Material properties and related dimensions.

Domain	Material	Density kg/m³	Specific heat j/kg · K	Thermal conductivity W/m · K	Viscosity kg/m · s	Dimensions mm
Tube	Carbon Steel Seamless Pipe (SA210 C)	7830	465	53	NA*	$D_o = 44.45$ $t_p = 5.588$ $L_p = 500$
Fluid	Water at $P = 210\ bar$ $T_{avg} = 369.83℃$	669.99	6181.4	0.51426	0.000078962	-

*NA refers to not applicable.

2.2. Numerical Model

2.2.1. Governing Equations

a comprehensive three-dimensional thermal model conjugate with an incompressible turbulent flow model is developed. To find out the thermo-fluid characteristics of the proposed heated water considering deposits layer. The governing equations include applying conservation of energy on solid parts and conservation of mass, momentum, and energy with turbulence model on fluid parts.

2.2.1.1. Solid Regions: Tube Wall and Deposits Layer

The conservation of energy governs the thermal characteristics and energy transfer through the solid domain, including the tube wall and deposits layer and can be written as follows:

- Conservation of Energy:

$$\nabla \cdot (k_s \nabla T) = 0 \tag{1}$$

Where k_s is the thermal conductivity of the solid part (i.e., tube material or deposits material), and the term on the left-hand side refers to the heat flux by conduction.

2.2.1.2. Fluid Region

The flow inside the tube is considered to be single-phase, steady, Newtonian, incompressible, and turbulent. Therefore, the flow characteristics can be represented using the conservation of mass, momentum-based on Reynolds-averaged Navier–Stokes (RANS) equations coupled with turbulence model, and conservation of energy as indicated by equations (2) to (7):

- Conservation of mass and momentum:

Preprints (www.preprints.org) | NOT PEER-REVIEWED | Posted: 17 June 2022 doi:10.20944/preprints202206.0254.v1

$$\frac{\partial \overline{u_\iota}}{\partial x_i} = 0 \tag{2}$$

$$\overline{u_\iota}\frac{\partial \overline{u_\iota}}{\partial x_i} = -\frac{1}{\rho_f}\frac{\partial \bar{P}}{\partial x_i} + \frac{\mu_f}{\rho_f}\frac{\partial^2 \overline{u_\iota}}{\partial {x_j}^2} - \frac{\partial}{\partial x_j}(\overline{{u_\iota}'{u_\iota}'}) \tag{3}$$

Where $\overline{u_\iota}$ and x_i refer to the mean velocity of the flow and coordinate system, respectively, with $i = 1, 2, and\ 3$. $\bar{P}$ is the mean pressure of the flow while ρ_f and μ_f represents water density and viscosity, respectively. $\overline{{u_\iota}'{u_\iota}'}$ is the turbulent Reynolds stress associated with the imposed turbulence over the mean flow, modelled and solved via turbulence models.

- Turbulence Model: Realizable k-ε turbulent model

the realizable k-ε turbulent model with enhanced wall function is used following Zhang, (2020) Zhouhang Li, (2014) to account for the existing fully turbulent flow with obtaining an accurate solution at a reasonable computational time. The model is based on model transport equations for the turbulence kinetic energy (k) and its dissipation rate (ε). The modeled transport equations for Realizable k-ε model for steady, incompressible, fully turbulent flow can be written as follows

$$\frac{\partial}{\partial x_j}(\rho_f k u_j) = \frac{\partial}{\partial x_j}\left[\left(\mu + \frac{\mu_t}{\sigma_k}\right)\cdot\frac{\partial k}{\partial x_j}\right] + G_k + G_b - \rho\varepsilon \tag{4}$$

and

$$\frac{\partial}{\partial x_j}(\rho_f \varepsilon u_j) = \frac{\partial}{\partial x_j}\left[\left(\mu + \frac{\mu_t}{\sigma_\varepsilon}\right)\cdot\frac{\partial \varepsilon}{\partial x_j}\right] + \rho_f C_1 S\varepsilon - \rho_f C_2 \frac{\varepsilon^2}{k + \sqrt{\upsilon\varepsilon}} + C_{1\varepsilon}\frac{\varepsilon}{k}C_{3\varepsilon}G_b \tag{5}$$

where

$$C_1 = max\left[0.43, \frac{\eta}{\eta + 5}\right], \eta = S\frac{k}{\varepsilon}, S = \sqrt{2S_{ij}S_{ij}} \tag{6}$$

where G_k and G_b refers to the generation of turbulence kinetic energy due to the mean velocity gradients and the generation of turbulence kinetic energy due to buoyancy, respectively. C_1 and $C_{1\varepsilon}$ are constants where σ_ε and σ_k are the turbulent Prandtl numbers for ε and k, respectively.

- Conservation of Energy:

$$\nabla\cdot(\vec{u}h) = \nabla\cdot(k_w\nabla T) \tag{7}$$

where h is the sensible enthalpy and equal to $\int_{T_{ref}}^{T} c_p dT$, and c_p is the specific heat at constant pressure.

2.2.2. Boundary Conditions

The applied boundary conditions are presented in Fig. 2. To reduce the computational costs, the quartile of the domain (i.e., water tube) is considered, and therefore, a symmetry boundary condition is applied on the XY and ZY planes, as indicated in Fig. 2. Instead of applying constant heat flux on the outer surface of the water tube following the literature (e.g., see references [15]), the combined heat transfer at the outer surface of the tube with flue gases undergoes a mixed convection and radiation heat transfer as follows:

$$Q_s = Q_{conv} + Q_{rad} = hA_s(T_{flue} - T_s) + \sigma\varepsilon A_s(T_{flue}^4 - T_s^4) \tag{8}$$

where T_{flue} and T_s are the flue gas and surface temperatures. A_s is the outer surface area of the water tube. σ is the Stefan Boltzmann constant, and ε is the emissivity of the outer surface of the pipe set to 0.8. h is the heat transfer coefficient which is varied in the present work between 100, 130, and 160 $W/m^2.K$ to represent different loads of 50%, 75%, and 100% considering approximated values from [16]. Besides, the flow gas temperature

Preprints (www.preprints.org) | NOT PEER-REVIEWED | Posted: 17 June 2022 doi:10.20944/preprints202206.0254.v1

is constant at 1500 K for all simulated cases except cases where the effect of flue gas temperature is highlighted, and the value ranges from 600 K to 1750K.

A thermally coupled boundary conditions are used at the interfaces, such as the interface between the inner surface of the water tube and the outer surface of the deposits layer and the interface between the inner surface of the deposits layer with water volume circumferential surface in the case of the tube with deposits layer. Moreover, the inlet and outlet are set to velocity inlet and pressure outlet boundary conditions, respectively. At the inlet, the constant mass flow rate is adopted equal to 0.3684kg/s, representing the total mass flow rate circulated between drums divided by the number of tubes. The Reynolds number for the presented cases beyond critical value and therefore turbulent flow model is considered. The inlet temperature of the water T_i is set to 290℃, the minimum temperature recommended at the operating pressure $P = 180 : 270$ bar. Nevertheless, the maximum value of the range, $P = 270$ bar, is considered in the present work, which leads to the minimum thickness attained under severe working conditions.

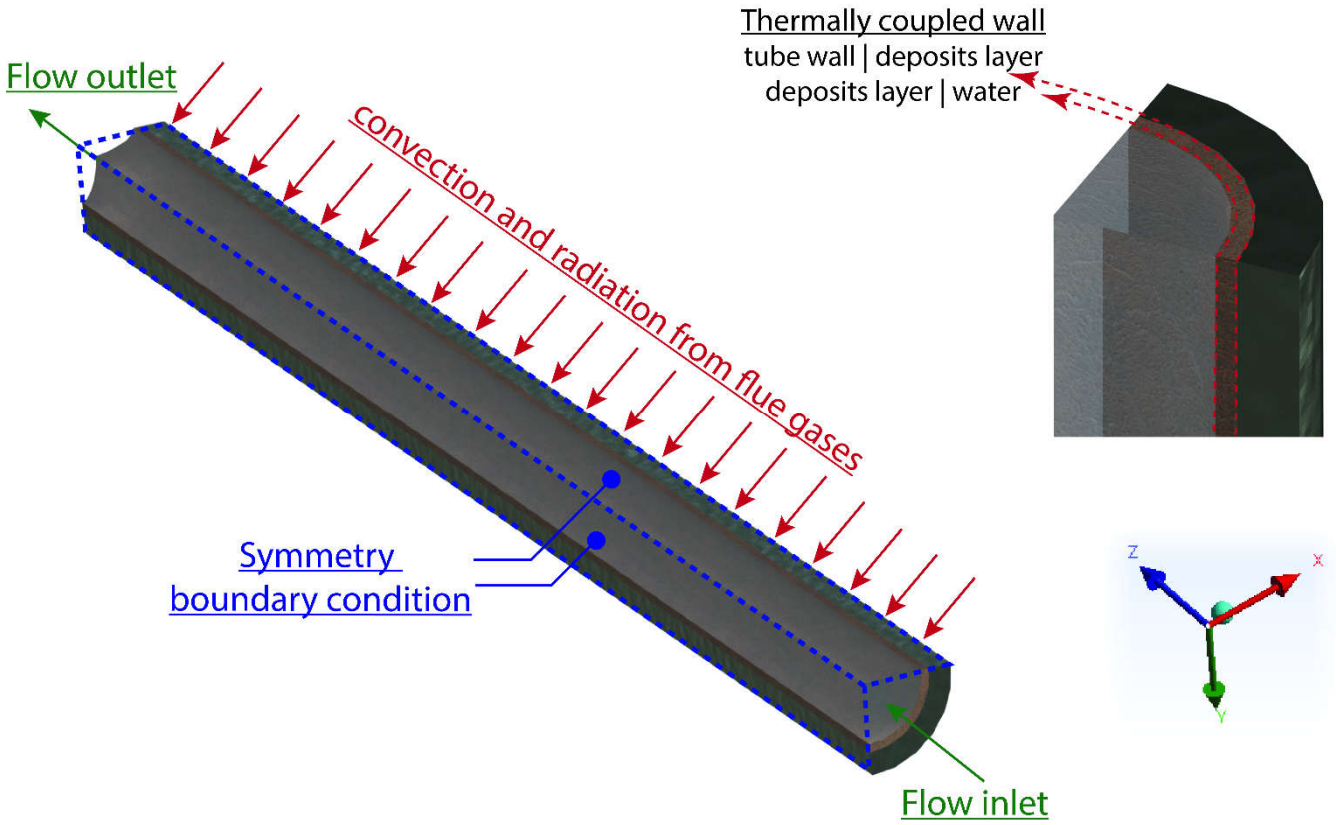

Figure 2. Boundary conditions on the simulated domain.

2.2.3. Minimum Tube Thickness Calculations (ASME)

The minimum thickness is determined using the following relation:

$$t_p = \frac{PD_o}{2\sigma + P} + 0.005D_o \tag{9}$$

Where P is the pressure inside the tube; D_o is the outer diameter of the water tube; σ is the allowable stress which is determined by two methods: (1) based on allowable stress from ASME code section II Part D for carbon steel seamless pipe (SA210 C) ASME, (2004) and (2) based on the strength σ_{max} of SA210 C from ASME code multiplied by a safety factor SF=4 usually considered in power plant applications. Note that both allowable stress and yield strength of carbon steel seamless pipe (SA210 C) are temperature-dependent, as shown in table 3.

Preprints (www.preprints.org) | NOT PEER-REVIEWED | Posted: 17 June 2022 doi:10.20944/preprints202206.0254.v1

Table 3. The maximum allowable stress and yield strength based on ASME code section II Part D for carbon steel seamless pipe (SA210 C) [17]

T [°C]	Maximum Allowable Stress, MPa	T [°C]	Yield Strength, MPa
40	138	40	276
65	138	65	259
100	138	100	251
125	138	125	248
150	138	150	244
200	138	175	240
250	138	200	237
300	138	225	232
325	138	250	227
350	135	275	221
375	123	300	216
400	101	325	209
425	83.8	350	202
450	67	375	196
475	51	400	191
500	33.6	425	185
525	21.3	450	180
550	12.9	475	176
		500	171
		525	167

2.3. Numerical Solution and Model Verification

2.3.1. Mesh Independence Test

The mesh has been created in water, deposits layer, and tube wall domains via ANSYS meshing. A mesh independence test is performed to exclude the influence of the mesh on the simulation calculations. Figure 3 shows the grid independence test for the water tube with deposits layer with multiple element sizing of 1, 0.8, 0.6, 0.4, 0.3 mm that attains a different number of mesh elements, as represented by 63900, 87300, 114200, 183400, and 259200 elements, respectively. Given the independence of maximum and average surface temperatures of the water tube on the mesh element at 183400, 0.4 mm element sizing has been chosen for being accurately sufficient with lower computational time.

Preprints (www.preprints.org) | NOT PEER-REVIEWED | Posted: 17 June 2022 doi:10.20944/preprints202206.0254.v1

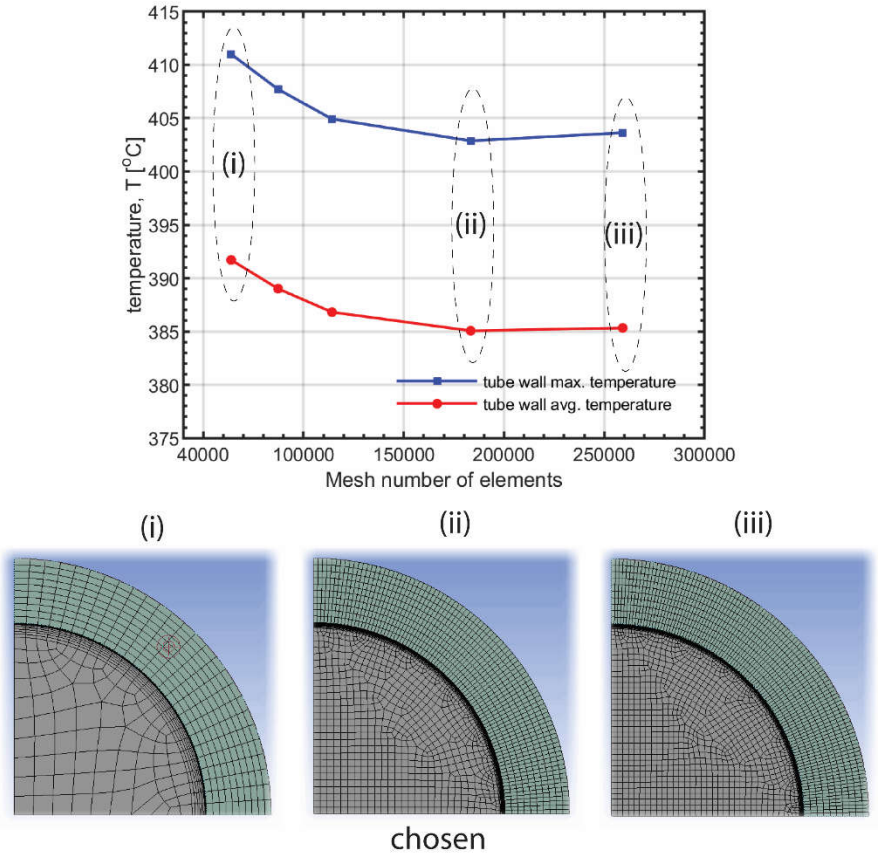

Figure 3. Mesh independence test.

3. Results and Discussion

3.1. Effect of Deposit Layer Thermal Conductivity at Different Load

In the present section, the estimation of minimum thickness via equation (9) that assures the safe operation of the water tubes in the furnace section of the boiler is determined, as indicated in Figure 4. Such calculations are based on the maximum temperature of the water tube wall (see Figure 4a) estimated from numerical simulation in ANSYS FLUENT [18]. Subsequently, such value of temperature is used to determine the yield strength via ASME Code (see Figure. 4b) and maximum allowable stress via either ASME Code (see Figure. 4c) or a constant safety factor SF=4 from the yield strength (see Figure. 4d) for carbon steel seamless pipe (SA210 C). Figure 4 highlights the effect of deposits layer thickness at a minimum thermal conductivity of different deposits layer presented in Table 2 (i.e., Magnetite), representing a severe scaling. Two minimum thicknesses are reported (see Figures 4e and f) due to obtaining allowable stress in two different techniques: variable safety factor as adopted in ASME Code or constant SF=4 practically employed in power plants.

As shown in Figure 4a, the accumulation deposits layer with low thermal conductivity is accompanied by an increasing the maximum temperature of the water tube wall. Such an increasing trend is at a low rate at relatively high thermal conductivity while being at high rates for deposits layer with thermal conductivity less than $k = 2\,W/mK$. For example, the maximum temperature T_{max} reaches 388.98, 394.33, and 402.92 ℃ at $k = 12.5W/mK$ compared with 484.99, 495.8, and 509.75 ℃ in the case of $k = 0.625\,W/mK$ for a different load of 50%, 75%, and 100%, respectively. Consequently, decreasing the thermal conductivity leads to a significant reduction in yield strength (Figure 4b), allowable stress based on ASME code (Figure 4c), or SF=4 (Figure 4d). Comparing the allowable stress via ASME code and the one via SF=4, it can be noticed that deposits layer

 doi:10.20944/preprints202206.0254.v1

with high thermal conductivity, i.e., $k = 12.5\ W/m\ K$, the allowable stress at full load reaches 989.92 and 475.7 bar, respectively, while it reaches 288.02 and 423.6 bar at $k = 0.625\ W/m\ K$, respectively. Such difference between the estimation of the allowable stress using ASME code or via constant safety factor of SF=4 is attributed to the use of ASME code. A variable safety factor increases with increasing the temperature. Consequently, this explains the difference between ASME code and using SF=4 to determine the minimum thickness of the tube wall (Figure 4e and f), in which lower values of the minimum thickness of water tube are proposed by ASME code for deposit layer with high thermal conductivity and vice versa for those with low thermal conductivity.

Overall, the maximum value of the estimated wall tube thickness is 12.1 mm, which is more than twice the original value considered in the present work. Therefore, chemical treatment is recommended for the water tubes in the case of the formation of a deposits layer with thermal conductivity less than 1~2 W/m K. Another temporal action is considering the operation at a lower load if being feasible till conducting the chemical treatment.

Preprints (www.preprints.org) | NOT PEER-REVIEWED | Posted: 17 June 2022 doi:10.20944/preprints202206.0254.v1

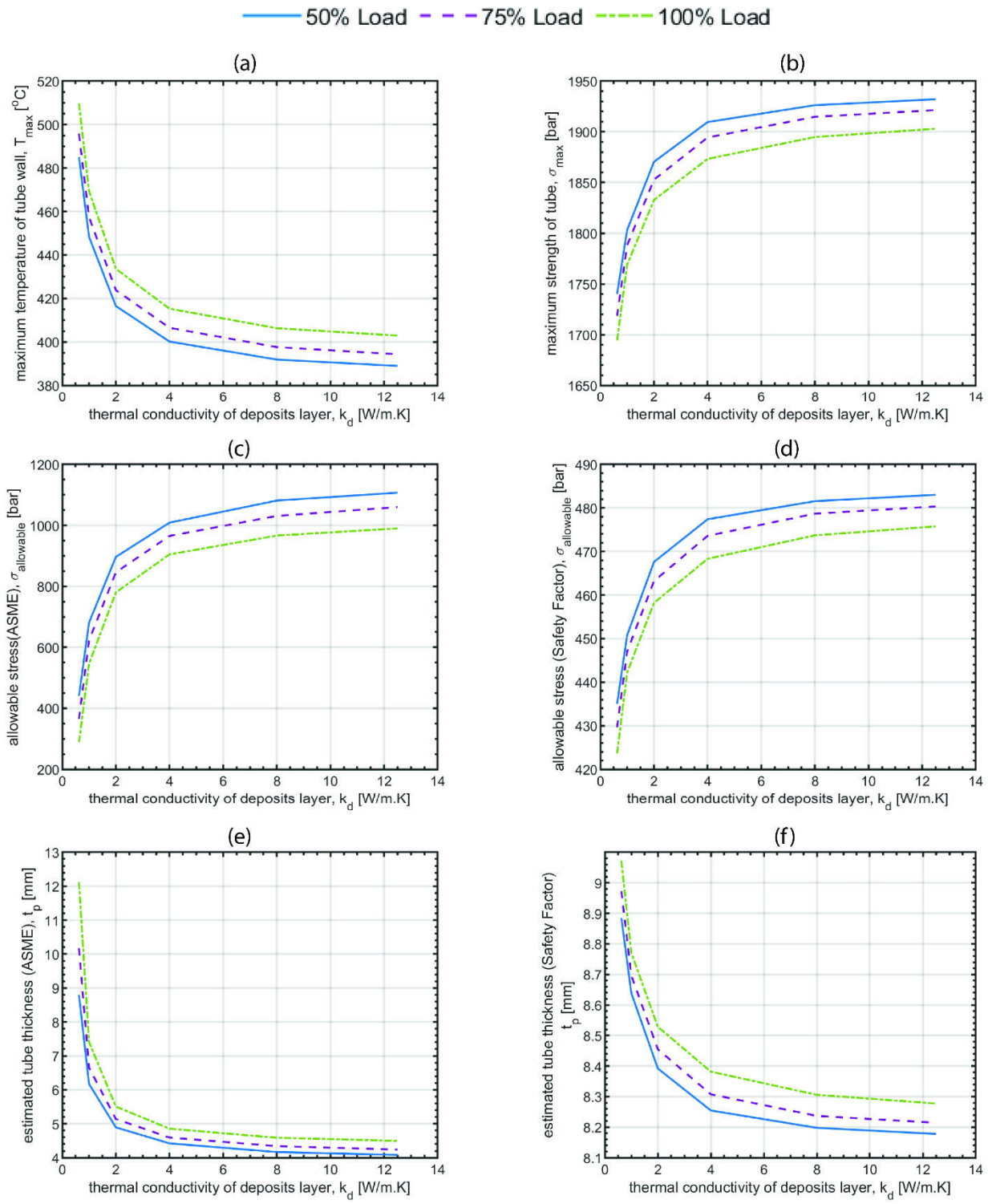

Figure 4. Thermal conductivity variation effects of deposits layer on (a) maximum temperature of the tube wall, (b) maximum yield strength of the water tube, (c) allowable stress based on ASME code, (d) allowable stress based on SF=4, (e) estimated tube thickness via ASME code, and (f) estimated tube thickness considering SF=4.

3.2. Effect of Deposit Layer Thickness at Different Load

A similar analysis, as previously discussed, is conducted in the present section to estimate the minimum thickness of the water tube to highlight the effect of the thickness

Preprints (www.preprints.org) | NOT PEER-REVIEWED | Posted: 17 June 2022 doi:10.20944/preprints202206.0254.v1

of the deposits layer, as shown in Figure 5. It is indicated that the increase of the deposits layer thickness leads to a linear increase in the maximum temperature of the water wall. In addition, increasing the load represented by the increase of the heat transfer coefficient between the water tube and flue gases results in a rise in the maximum temperature of the tube wall. As a result, a linear reduction is monitored for yield strength (Figure 5b) and allowable stress (Figures 5c and d) by increasing the deposits layer's thickness. Consequently, the minimum thickness of the tube based on equation (9) increases with the increase of deposits layer thickness (Figures 5e and f). Such increase exhibits a linear trend in the case of the use of allowable stress based on a constant safety factor of SF=4 (Figure 5f) while showing a nonlinear trend in the case of the use the allowable stress based on the ASME code (Figure 5e) due to the increasing SF with the temperature.

Note that a higher thickness of the water tube for safe operation is attained using allowable stress with constant SF=4 (Figure 5f) at a small thickness of deposits layer compared with that attained by ASME Code (Figure 5e), and the reverse occurs at a higher thickness of the deposits layer thickness. For example, the estimated minimum thickness reaches $12.1mm$ at the highest allowable thickness of $172\ \mu m$ (Table 1), which is twice higher than the originally adopted value. Consequently, using tube thickness less than $12.1mm$ suggests cautious monitoring of deposits layer thickness to avoid a high potential of overheating occurrence in the case of minimum thermal conductivity of deposits layer (e.g., Magnetite).

Preprints (www.preprints.org) | NOT PEER-REVIEWED | Posted: 17 June 2022 doi:10.20944/preprints202206.0254.v1

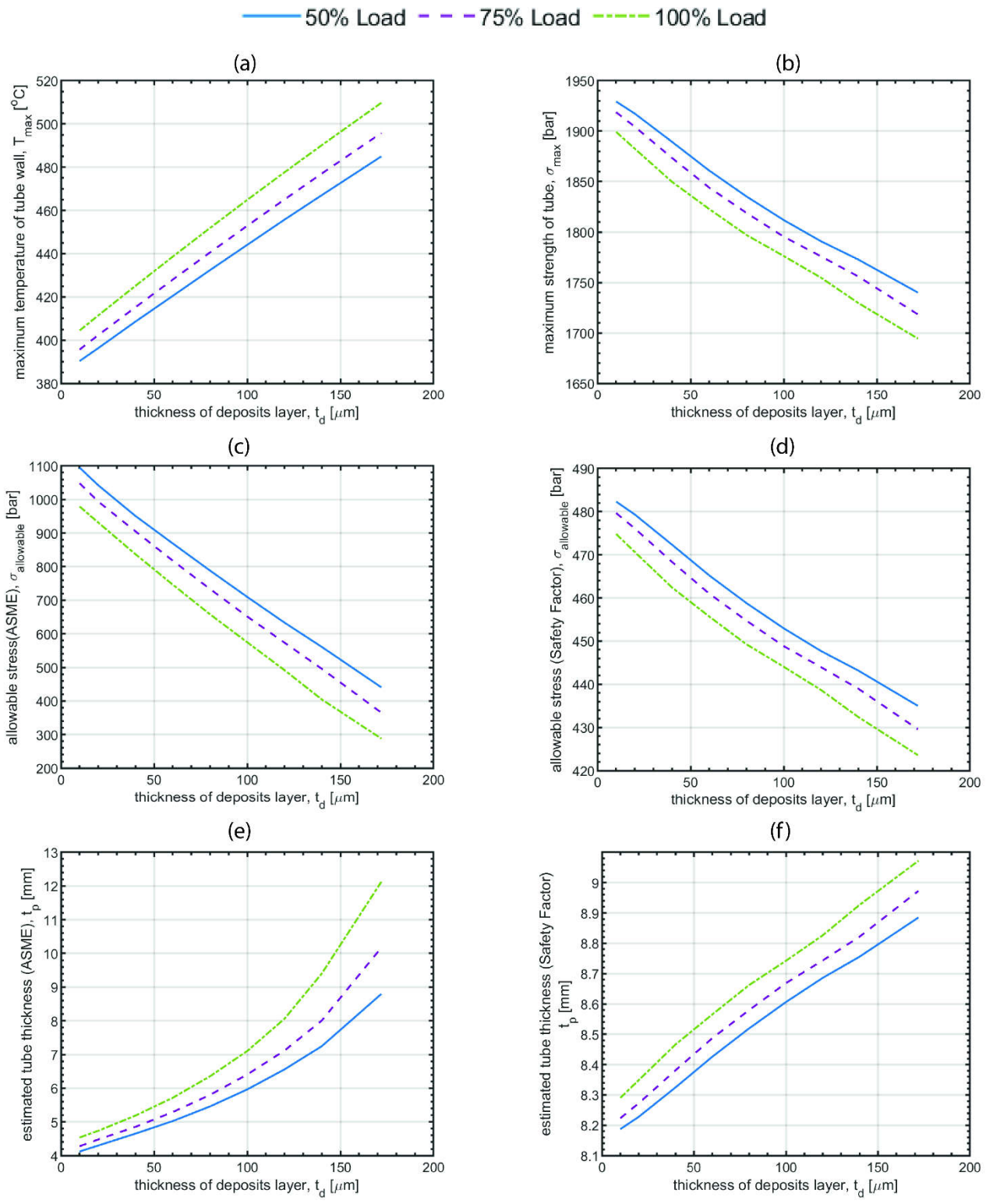

Figure 5. Thickness variation effects of deposits layer on (a) maximum temperature of the tube wall, (b) maximum yield strength of the water tube, (c) allowable stress based on ASME code, (d) allowable stress based on SF=4, (e) estimated tube thickness via ASME code, and (f) estimated tube thickness considering SF=4.

 doi:10.20944/preprints202206.0254.v1

3.3. Effect of Flue Gas Temperature at Different Load

Finally, as shown in Figure 6, the effect of the flue gas temperature on the maximum temperature of the tube, yield strength of the water tube, allowable stress, and the estimated tube minimum thickness is highlighted in the current section to mimic the effect different source flue gases such as different burning fuel, or exhaust from equipment such as a gas turbine.

As indicated by Figure 6a, the increase in the flue gas temperature results in a significant increase in the maximum wall tube temperature up to 827.5342 ℃ at a flue gas temperature of 1726.85 ℃, which is much higher than the values of 525 ℃ and 550 ℃ (See table 3) maximumly recommended for yield strength and allowable stress respectively by ASME code for carbon steel seamless pipe (SA210 C). Therefore, increasing the flue gases in the furnace section beyond 1226.9 ℃ (1500 K) is not recommended, and the subsequent effects of flue gases on yield strength, allowable stress, and minimum thickness are limited to 1226.9℃, as shown in Figure 6b-f. Note that allowable stress based on ASME code is high at lower flue gas temperature with a slight decrease up to 728℃, beyond which sudden drop is encountered following the interpolated values of the wall tube maximum temperature in Table 3. Accordingly, the minimum thickness (Figure 6e) slightly increases up to 728℃, beyond which a sudden rise is observed. Based on the originally used thickness of the water tubes in the present work, the water tubes can resist the overheating for lowest thermal conductivity and the maximum thickness of the deposit layers up to 850℃ of flue gases working at 100% load. After such values, the minimum thickness of the water tube wall needs to increase to higher values reaching $11.97mm$ at 1226.9 ℃. It is worth mentioning that, considering allowable stress with Constant SF=4 (Figure 6f), the minimum thickness compared with that of ASME-based is higher at low flue gases temperature and vice versa at high flue gases temperature.

Preprints (www.preprints.org) | NOT PEER-REVIEWED | Posted: 17 June 2022 doi:10.20944/preprints202206.0254.v1

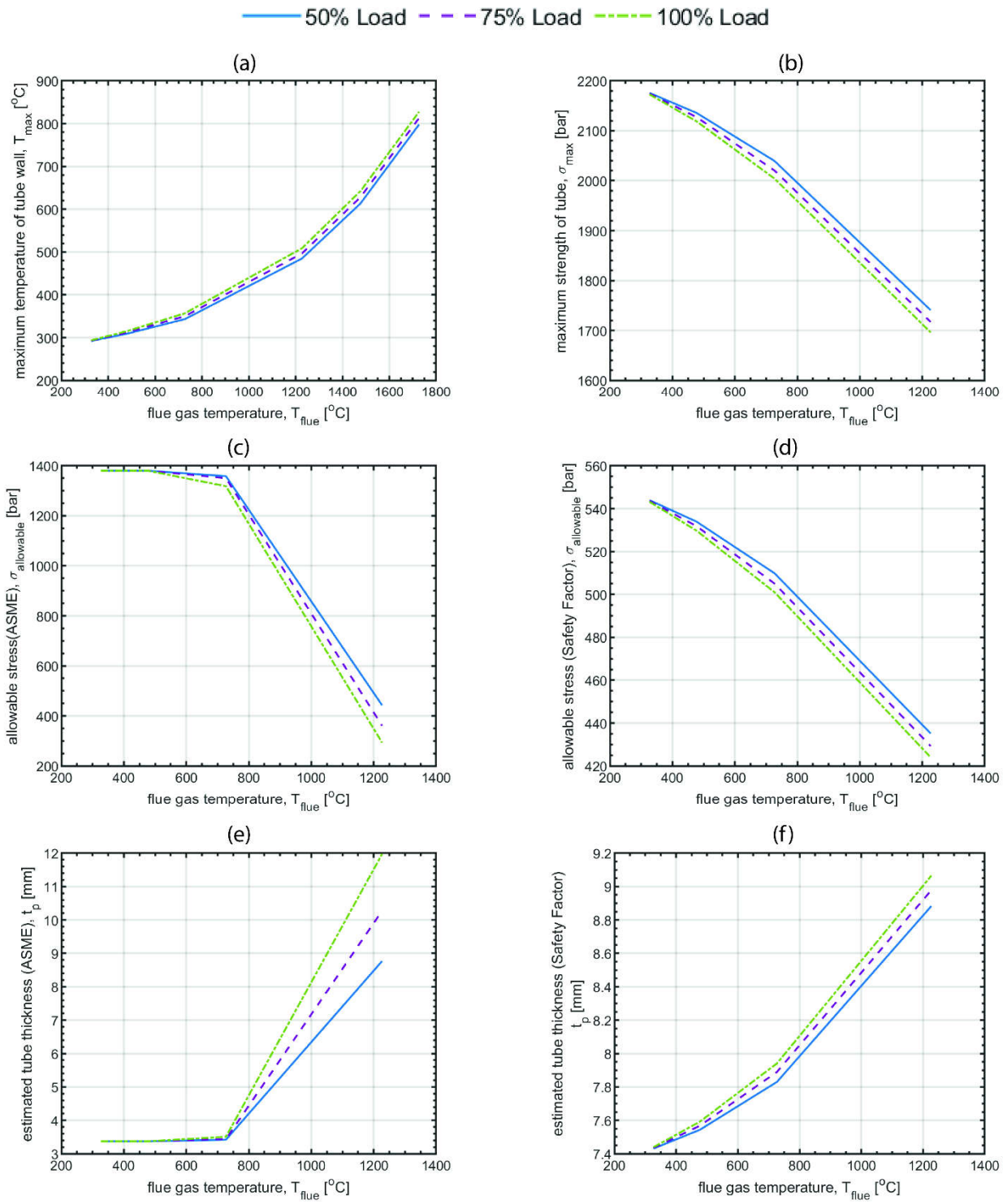

Figure 6. Effects of flue gases temperature variation on (a) maximum temperature of the tube wall, (b) maximum yield strength of the water tube, (c) allowable stress based on ASME code, (d) allowable stress based on SF=4, (e) estimated tube thickness via ASME code, and (f) estimated tube thickness considering SF =4.

5. Conclusions

The present work was set to numerically determine the effect of the deposit layer thickness and thermal conductivity on the minimum thickness of the tube wall that attains

 doi:10.20944/preprints202206.0254.v1

safe operation considering the different working loads of 50%, 75%, and 100% at the maximum operating working pressure of 210 bar. Based on the adopted parameters, the investigation of the minimum thickness of the water tube wall has revealed that:

1- The thermal conductivity of deposits affects the maximum temperature of the tubes. Consequently, the high potential for overheating, particularly at the deposits layer with thermal conductivity less than $k = 1$ W/m K. For example, considering $k = 0.625$ W/m.K, the maximum temperature exceeds 500°C at 100% load, proposing more than double the tube's original thickness for safe operation according to ASME Code for maximum allowable stress for carbon steel seamless pipe (SA210 C).

2- Increasing the thickness of the deposits layer leads to a linear increase of tube wall maximum temperature. For the lowest thermal conductivity in the present work (i.e., Magnetite), safe operation is obtained within the accumulation of deposits layer up to 50 μm. Beyond this value, the designer or the operator needs to consider thicker tubes which might lead to more than double the original thickness of the current work. Consequently, it is essential to consider the consistency between the chosen wall tube thickness and the maintenance schedule considering the deposits accumulation rates and the operating conditions.

3- The flue gas temperature, representing different sources of burned fuels or exhausts from gas turbines in combined power plants, significantly increases the minimum thickness of the water tubes, particularly beyond 725°C. In addition, the flue gas temperature is not recommended beyond 1225.9°C (1500 K), as the corresponding maximum water tube temperature exceeds those values provided by the ASME code for maximum allowable stress.

The present study is limited to the water tube in the furnace section. The identified effect of the deposits layer on the tube wall temperature and the corresponding minimum thickness in terms of thickness and thermal conductivity at different operating conditions assists our understanding of the role of the deposits layer attributes for suitable selection of the tube thickness and courses of action concerning the operating conditions that minimize the potential overheating of water tubes in the furnace section of the boiler.

References

[1] G. F. J. Melville, "A pictorial review of failures in conventional boiler plant," *Pressure Vessels and Piping,* vol. 3, no. 1, pp. 1-25, 1975.

[2] E. E. J. C. M. Camilo A. Duarte, "Failure analysis of the wall tubes of a water-tube boiler," *Engineering Failure Analysis,* vol. 79, pp. 704-713, 2017.

[3] A. A. N. A. S. M. M.R. Khajavi, "Failure analysis of bank front boiler tubes," *Engineering Failure Analysis,* vol. 14, no. 4, pp. 731-738, 2007.

[4] D. e. a. Ghosh, "Failure Analysis of Boiler Water Wall Tube: A Case Study from Thermal Power Plant," *Failure Analysis and Prevention,* pp. 1-6, 2022.

[5] R. A. e. a. Himarosa, "Failure analysis of platen superheater tube, water wall tube, and sealpot plate: A case study from electricity power plant in indonesia," *Engineering Failure Analysis,* vol. Volume 135, pp. 106-108, 2022.

[6] J. Taler, P. Dzierwa, M. Jaremkiewicz, D. Taler, K. Kaczmarski, M. Trojan and T. Sobota, "Thermal stress monitoring in thick walled pressure components of steam boilers," *Energy,* pp. 645-666, 2019.

[7] L. Sun and W. Yan, "Prediction of wall temperature and oxide scale thickness of ferritic–martensitic steel superheater tubes," *Applied Thermal Engineering,* pp. 171-181, 2018.

[8] N. Modliński, K. Szczepanek, D. Nabagło, P. Madejski and Z. Modliński, "Mathematical procedure for predicting tube metal temperature in the second stage reheater of the operating flexibly steam boiler," *Applied Thermal Engineering,* pp. 854-865, 2019.

[9] H. Ardy and D. A. Bangun, "Failure Analysis of Superheater Boiler Tube SA 213 T12," in *IOP Conference Series: Materials Science and Engineering*, Bandung, Indonesia, 2019.

[10] F. Dehnavi, A. Eslami and F. Ashrafizadeh, "A case study on failure of superheater tubes in an industrial power plant," *Engineering Failure Analysis,* pp. 368-377, 2017.

[11] G. P. S. M. K. A. K. P. Bipin Kumar, "A review of heat transfer and fluid flow mechanism in heat exchanger tube with inserts," *Chemical Engineering and Processing - Process Intensification,* vol. Volume 123, pp. Pages 126-137, 2018.

[12] M.C.Barma, R.Saidur, S.M.A.Rahman, A.Allouhi, B.A.Akash and S. M.Sait, "A review on boilers energy use, energy savings, and emissions reductions," *Renewable and Sustainable Energy Reviews,* pp. 970-983, 2017.

[13] Sadik Kakaç, H. Liu and A. Pramuanjaroenkij, Heat Exchangers: Selection, Rating, and Thermal Design, Fourth Edition, CRC Press, 2020.

[14] N. T. Mohite and R. G. Benni, "Optimization of Wall Thickness for Minimum Heat Losses for Induction Furnace," *International Journal of Engineering Research and Technology,* pp. 645-653, 2017.

[15] Z. L. L. W. L. L. N. L. Q. Z. C. M. Jiapeng Fu, "Identification of the running status of membrane walls in an opposed fired model boiler under varying heating loads," *Applied Thermal Engineering,* vol. Volume 173, p. 115217, 2020.

[16] H. B. P. M. Jagodzińska K, "An analysis of coal and coal mine methane co-combustion in an 140 t/h pulverized coal boiler," *Transactions of the Institute of Fluid-Flow Machinery,* pp. 3-18, 2017.

[17] ASME, Pressure Vessel Code, New York: ASME, 2004.

[18] FLUENT, Theory Guide, ANSYS, 2021.

[19] Z. Z. Y. H. N. L. X. J. Y. a. Y. H. Zhang, "A thermal stress analysis of fluid–structure interaction applied to boiler water wall," *Asia-Pacific Journal of Chemical Engineering,* vol. 15, no. 6, p. e2537, 2020.

[20] Y. W. J. L. D. Z. H. Z. Zhouhang Li, "Heat transfer to supercritical water in circular tubes with circumferentially non-uniform heating," *Applied Thermal Engineering,* vol. 70, no. 1, pp. Pages 190-200, 2014.

[21] P. Munda, M. M. Husain, V. Rajinikanth and A. K. Metya, "Evolution of Microstructure During Short-term Overheating Failure of a Boiler Water Wall Tube Made of Carbon Steel," *Failure Analysis and Prevention,* no. 18, pp. 199-211, 2018.

[22] Y. Hu, HailongLi and J. Yan, "Numerical investigation of heat transfer characteristics in utility boilers of oxy-coal combustion," *Applied Energy,* pp. 543-551, 2014.

[23] P. Munda, M. M. Husain, V. Rajinikanth and A. K. Metya, "Evolution of Microstructure During Short-term Overheating Failure of a Boiler Water Wall Tube Made of Carbon Steel," *Journal of Failure Analysis and Prevention, 18(1),* p. 199–211, 2018.